50 In Vivo Optical Microendoscopy for Imaging Cells Lying Deep within Live Tissue

Robert P.J. Barretto[1] and Mark J. Schnitzer[1,2]

[1]James H. Clark Center for Biomedical Engineering & Sciences, Stanford, California 94305; [2]Howard Hughes Medical Institute, Stanford University, Stanford, California 94305

ABSTRACT

Although in vivo microscopy has been pivotal in enabling studies of neuronal structure and function in the intact mammalian brain, conventional intravital microscopy has generally been limited to superficial brain areas such as the olfactory bulb, the neocortex, or the cerebellar cortex. For imaging cells in deeper areas, this chapter presents in vivo optical microendoscopy using gradient refractive index (GRIN) microlenses that can be inserted into tissue. The methodology we present is described in detail for the CA1 hippocampal area, but our general approach is broadly applicable to other deep brain regions and areas of the body. Microendoscopes are available in a wide variety of optical designs, allowing imaging across a range of spatial scales and with spatial resolution that can now closely approach that offered by standard water-immersion microscope objectives. Microendoscopes are also compatible with chronic animal preparations that permit longitudinal imaging studies of deep brain tissues. The incorporation of microendoscope probes into portable miniaturized microscopes allows imaging in freely behaving animals. When combined with the broad sets of available fluorescent markers, animal preparations, and genetically modified mice, the methods described here enable sophisticated experimental designs for probing how cellular characteristics may underlie or reflect animal behavior and life experience, in healthy animals and animal models of disease.

INTRODUCTION

Recent strides in intravital light microscopy have enabled seminal studies of both neuronal structure and dynamics in the intact mammalian brain (Gobel and Helmchen 2007; Kerr and Denk 2008; Rochefort et al. 2008; Holtmaat et al. 2009; Holtmaat and Svoboda 2009; Wilt et al. 2009). Applications of two-photon microscopy in awake but head-restrained animals have even permitted Ca^{2+}-imaging studies during active animal behavior (Dombeck et al. 2007; Mukamel et al. 2009; Nimmerjahn et al. 2009). However, photon scattering limits the optical penetration of light

microscopy into tissue, restricting the utility of conventional intravital microscopy to superficial tissue areas such as the olfactory bulb, the neocortex, and the cerebellar cortex (Helmchen and Denk 2005; Wilt et al. 2009). Penetration depths are typically limited to ~50–100 μm with epifluorescence microscopy and ~500–700 μm with conventional two-photon microscopy.

To extend the microscope's penetration depth into tissue, a range of innovative optical strategies has been experimentally explored in the last few years (Helmchen and Denk 2005; Wilt et al. 2009). Here, we describe one of these approaches: optical microendoscopy (Jung and Schnitzer 2003; Jung et al. 2004; Levene et al. 2004), which can penetrate the furthest of these and reach >1 cm into tissue (Llewellyn et al. 2008) via the use of needle-like micro-optical probes. These probes typically act like an optical relay and can be inserted into tissue. Subject to some optical constraints discussed below, the length of the probe can be tailored to the anatomical depth of the tissue under examination. Optical microendoscopy provides spatial resolution that can approach that of a conventional water-immersion objective lens (Barretto et al. 2009); is compatible for use with multiple contrast modalities including epifluorescence, two-photon excited fluorescence, and second-harmonic generation (Mehta et al. 2004; Flusberg et al. 2005); and has been used in both live mice and humans (Llewellyn et al. 2008; Wilt et al. 2009). In this protocol, we present optical considerations in the choice of a microendoscope probe, modifications to the upright light microscope that facilitate microendoscopy, and a chronic animal preparation that permits long-term time-lapse imaging of cellular characteristics in the intact mammalian brain. This preparation is also compatible for use with portable miniaturized microscopes (Gobel et al. 2004; Engelbrecht et al. 2008; Flusberg et al. 2008) that are based on micro-optics and enable imaging in freely behaving mice (Flusberg et al. 2008).

IMAGING SETUP

Microscope Body

Nearly any upright microscope that has infinity optics and has already been adapted for in vivo imaging (e.g., Ultima IV, Prairie Technologies, Inc.) can readily be used for microendoscopy. There are two main options for how the microendoscope probe can be held (Barretto et al. 2009), one of which requires custom modifications to the microscope.

In the simpler approach, the microendoscope probe is held by its insertion into the animal subject, instead of being coupled mechanically to the body of the microscope. When the animal and the microendoscope probe are positioned correctly, the microendoscope relays the focal plane of the microscope objective into deep tissue, with a demagnification or magnification that depends on the optical details of the probe. This approach has the advantage of not requiring any alterations to the microscope but the disadvantage that any fine adjustments of the microendoscope relative to the tissue are not automatically referenced to the optical axis.

In an alternative approach, the microendoscope probe is mounted on the microscope's focusing unit, which is modified to permit two modes of fine focal adjustment (**Fig. 1A,C**). The first mode adjusts the position of the microscope objective lens relative to the microendoscope probe. The second mode moves the objective lens and the microendoscope probe in tandem, permitting the microendoscope to be inserted into tissue without affecting the optical coupling to the objective lens. Both modes can be motorized. To grip the microendoscope probe on its sides, we use a two-pronged pincer holder (e.g., Thorlabs, Inc., Micro-V-Clamp) (Fig. 1C). This holder is attached to a miniature probe clamp (e.g., Siskiyou, Inc., MXC-2.5) that can be rotated about its long axis and swung in and out of the optical pathway. By adjusting the two angular degrees of freedom of the probe clamp, we align the microendoscope with the optical axis (Barretto et al. 2009). Adjustments in the axial position of the objective lens while keeping the microendoscope fixed are performed using a stepper motor (Sutter Instruments, MP-285) mounted on the microscope's nosepiece. These adjustments modify the intermediate plane at which the illumination is focused above the microlens, leading to corresponding focal adjustments in the specimen. The microendoscope and objective lens are moved in tandem using the microscope's normal focusing actuator (Fig. 1C).

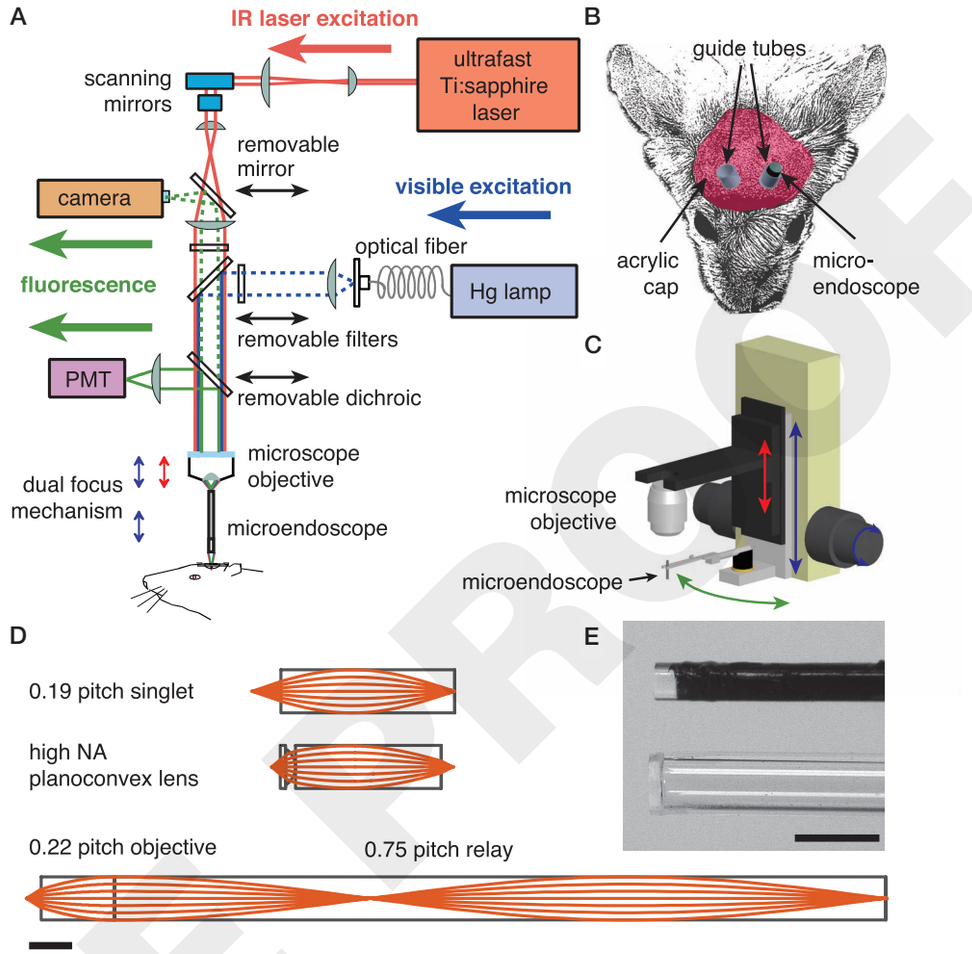

FIGURE 1. Methodologies for in vivo optical microendoscopy. (*A*) Optical schematic of an upright microscope modified to permit both one- and two-photon fluorescence microendoscopy. For two-photon imaging, the beam from an ultrashort-pulsed infrared (IR) Ti:sapphire laser is scanned within the focal plane of the microscope objective. By adjusting the axial separation between the objective and the microendoscope (red arrow of the dual-focus mechanism; see also *C*), this focal plane of the microscope objective is also set to the microendoscope's back focal plane. Another focal adjustment (blue arrows of the dual mechanism) is used to lower the objective and the microendoscope in tandem toward the animal. For one-photon imaging, a mercury (Hg) arc lamp provides illumination. In both imaging modes, fluorescence emissions route back through the microendoscope and to either a camera or a photomultiplier tube (PMT) for one- or two-photon imaging, respectively. (*B*) Guide tubes are surgically implanted into the rodent brain, allowing microendoscopes to be positioned just outside the brain area of interest. (*C*) The microscope objective and the microendoscope probe are mounted on a pair of cascaded focusing actuators that provide dual-focus capability. This allows the objective to be moved either alone (red arrow) or together with the microendoscope (blue arrow). The microendoscope can also be swung out of the optical axis (green arrow) to permit conventional microscopy. (*D*) Optical ray diagrams for sample microendoscopes of the singlet GRIN (*top*), compound plano-convex and GRIN (*middle*), and GRIN doublet (*bottom*) types. (*E*) Photographs of the tips of a 0.5-mm-diameter microendoscope of doublet design (*top*) and a 0.8-mm-outer-diameter glass guide tube (*bottom*) into which this microendoscope can be inserted. The relay of the microendoscope is coated black. The guide tube is sealed with a glass coverslip, providing optical but not physical access to the tissue.

Microendoscope Probes

Microendoscope probes can be customized for specific applications (Fig. 1D), and distinct values of the probes' basic optical parameters are preferred in different situations. For example, some optical designs are better suited for examining subcellular features such as dendritic structures, whereas other designs are preferred for wide-field Ca^{2+} imaging of neuronal dynamics. In our own work, we

TABLE 1. Characteristics of sample microendoscope probes

Microendoscope type	Diameter (mm)	Length (mm)	Usable field of view (µm)	Lateral magnification) (×)	Two-photon lateral resolution (FWHM, µm)	NA
Doublet (0.75/0.21 pitch)	1.0	20.6	275	2.52	0.9	0.49
Doublet (1.25/0.19 pitch)	0.5	16.4	130	2.48	1.0	0.48
Doublet (1.75/0.16 pitch)	0.35	15.8	75	2.69	1.2	0.45
Singlet (0.46 pitch)	1.0	4.4	700	0.97	0.9	0.49
Singlet (0.94 pitch)	0.5	4.3	350	0.92	1.0	0.47
GRIN/plano-convex doublet (BK7 plano-convex lens)	1.0	3.7	120	1.41	0.8	0.65
GRIN/plano-convex doublet (LaSFN9 plano-convex lens)	1.0	4.0	75	1.86	0.6	0.82

To facilitate comparisons between parameter values, each microendoscope listed has an optical working distance of 250 µm. The lateral resolution of two-photon imaging is given for 920-nm illumination.

FWHM, full width at half-maximum; NA, numerical aperture; GRIN, gradient refractive index.

have explored three main types of optical designs. The first design involves a single GRIN lens (Fig. 1D, top) that provides low magnification and a large field of view. The second design involves a GRIN lens attached in series to a high-numerical-aperture (NA) (~0.65–0.78) plano-convex microlens (Barretto et al. 2009) (Fig. 1D, middle); this combination can provide superior light collection and diffraction-limited resolution but has a smaller field of view. The third design has a GRIN relay lens coupled to a GRIN objective (Fig. 1D, bottom), allowing longer probe designs (>5 mm) and intermediate-sized fields of view (Jung et al. 2004; Levene et al. 2004).

Microendoscope probes of all three types (Fig. 1D, **Table 1**) can generally be conceptualized as consisting of two optical components in series: an infinity micro-objective that focuses illumination to the specimen and collects emission photons combined with a micro-optical relay lens that receives focused illumination from the microscope and also focuses the sample's emissions to the front focal plane of the upright microscope's objective lens (Fig. 1A,C). In singlet GRIN lenses, both of these functions occur within a single optical element; in GRIN doublet probes or in high-resolution probes, the jobs of the objective and the relay are accomplished by two micro-optical entities attached in series. In epifluorescence microendoscopy, the relay microlens projects a real image of the sample to the microscope objective's focal plane. Table 1 presents optical parameters for some microendoscopes, with each of the three major types represented. Below, we consider these parameters in further detail. For mathematical formulas to guide optical design, see Jung et al. (2004); with these equations researchers can design probes to custom specifications and have them fabricated commercially.

Microendoscope Diameter

Microendoscope probes with diameters ranging from 0.35 to 2.8 mm are commercially available (e.g., from GRINTECH GmbH); our laboratory most commonly uses 0.35-, 0.5-, and 1.0-mm sizes. For a given NA value, the smaller diameter probes (e.g., 0.35 or 0.5 mm) offer resolution and magnification values comparable to those of wider diameter probes. However, the wider probes of the same NA will generally have longer working distances to the sample and broader fields of view. In addition, smaller diameter probes are more fragile. Encasing these probes in thin-walled stainless-steel hypodermic sheaths will make them more robust. Probes as thin as 0.35 mm in diameter have been successfully applied for high resolution in vivo laser-scanning imaging, including in humans (Llewellyn et al. 2008).

Microendoscope Length

The lengths of microendoscope probes are typically designed to meet the mechanical constraints posed by the depth of the tissue under examination and the surgical preparation. The probe length should be sufficient to guide photons from the specimen plane lying deep within the tissue to an

unobstructed intermediate focal plane that is also the focal plane of the microscope objective (Fig. 1A). It is the length of the relay microlens that is typically adjusted in applications requiring imaging at substantial tissue depths.

Valid lengths for the relay microlens are calculated by first determining the pitch length of its glass GRIN substrate (Jung et al. 2004). Within a paraxial approximation, light rays propagate down the optical axis of the microendoscope along a trajectory for which the rays' radial distance from the axis varies as a sinusoidal function of the distance propagated axially (Fig. 1D). One pitch length is defined as the length of the GRIN substrate within which a ray will propagate a full sinusoidal cycle. This length depends on the radially varying refractive index profile of the GRIN material. Cylindrical rods of this material can then be cut to various lengths measured in units of the pitch length. GRIN lenses of integral or half-integral pitch—that is, 1/2, 1, 3/2 pitch, etc.—refocus light rays emanating from a single focus on one side of the lens to another focal spot on the opposite side of the lens. By comparison, 1/4-pitch lenses—or 3/4-pitch lenses, 5/4-pitch lenses, etc.—are infinity lenses that focus collimated rays entering one side of the microlens to a focal spot on the lens's opposing side (see the 0.75-pitch relay in Fig. 1D, bottom). Longer microendoscope probes can be designed by adding multiple 1/2-pitch lengths to the relay lens as necessary. Such additions extend the probe's length without altering the NA, the magnification, the field of view, or the working distance. However, probes of longer length often suffer from poorer optical resolution caused by the accumulation of spherical aberrations over multiple half-pitch lengths of the GRIN substrate.

Optical Working Distance to the Specimen

The working distance to the specimen is set for a GRIN objective lens by the degree to which the objective is slightly shorter than a 1/4-pitch design (see the 0.19-pitch singlet and the 0.22-pitch objective in Fig. 1D). An objective of shorter pitch has a longer working distance, but the objective's NA is reduced. Typical values of working distance range from 0 μm to 800 μm. In one-photon fluorescence imaging, light scattering precludes efficient imaging beyond ~100 μm from the tip of the endoscope (Flusberg et al. 2008), so the working distance will be relatively short. By comparison, in two-photon imaging, microendoscopy can be performed up to ~650 μm into tissue beyond the probe tip, which generally necessitates a design of longer working distance (Barretto et al. 2010). Although the focal plane can be adjusted to a depth other than the working distance, microendoscopes are often designed to have minimal optical aberrations at their specified working distance. In particular, the high-resolution GRIN/plano-convex compound lenses (Fig. 1D, middle) are designed so that aberrations from the objective component are compensated at a specific working distance by an appropriate choice of the GRIN relay's radial refractive index profile (Barretto et al. 2009). High-resolution experiments should, thus, be performed with the tissue of interest located at the designed working distance. However, for imaging experiments that permit modest degradation in resolution, it is convenient to design the optical working distance to be a few hundred micrometers longer than what will be used for the experiment. This choice ensures that neither the plane of laser scanning in two-photon imaging nor the intermediate real image in one-photon imaging is located at external glass surfaces of the microendoscope, where surface imperfections can degrade image quality.

Microscope Objectives for Optical Coupling to the Microendoscope Probe

Microscope Objective Magnification

In applications requiring large fields of view, the magnification of the microscope objective should suffice to permit imaging of the entire top surface of the microendoscope probe. For example, a typical 10x objective has a sufficient field of view to image the entire aperture of a 1-mm-diameter microendoscope probe. Other parameters of the entire optical system must also suffice to image this entire aperture. For example, in one-photon microendoscopy, the camera chip must be sufficiently wide; and in two-photon microendoscopy, the range of laser scanning must be sufficiently broad to sample the entire face of a 1-mm-diameter microendoscope probe.

Microscope Objective NA

To achieve high-resolution imaging, the NA of the microscope objective should be higher than that of the microendoscope probe's relay lens. In one-photon imaging, this condition ensures that the microscope objective captures the full NA of fluorescence emissions exiting the microendoscope's relay lens, thereby preserving signal power as well as image resolution. In two-photon imaging, this condition ensures that the laser illumination fills the back aperture of the probe's objective lens, typically located at the boundary between the micro-objective and the relay (Fig. 1D) and thereby uses the full NA of the microendoscope's objective in focusing the laser beam at the specimen plane. A portion of the laser illumination will be lost, however, because the NA of the beam striking the relay lens is higher than the NA that the relay can accept.

Imaging Parameters

One-Photon Imaging

Excitation filter: Approximately 470/40 nm for fluorescein-conjugated dextrans (for blood-flow imaging), green fluorescent protein (GFP) and yellow fluorescent protein (YFP).

Emission filters: Approximately 525/50 nm for fluorescein-conjugated dextrans, GFP, and YFP.

Images/frame rate: 512 × 512 pixels at 100 Hz with a high-speed electron-multiplying charge-coupled device (CCD) camera (e.g., iXon DU-897E, Andor Technology), or 1392 × 1040 pixels with a cooled CCD camera (e.g., Coolsnap HQ, Roper Scientific GmbH).

Recording duration: Typically 30–40 sec for a given field of view.

Two-Photon Imaging

Excitation wavelength: Approximately 800 nm for fluorescein-conjugated dextrans in vascular imaging, ~920 nm for GFP and YFP.

Excitation power at sample surface: Always <25 mW for tissues proximal to the microendoscope, more distal tissues require greater power.

Images/dwell times: 512 × 512 pixels (typically ~0.8–4 μsec per pixel or as permitted by tissue motion). For high-resolution imaging, multiple images can be acquired and can be averaged, after motion correction, to produce an improved image.

Section/stack (3D imaging): Approximately 5–10-μm axial spacing for GRIN singlets and doublets that have ~10-μm axial resolution, 1–2.5-μm axial spacing for high-resolution microlenses.

Recording duration: Typically 5–10 min for a given field of view.

Protocol

In Vivo Microendoscopy of the Hippocampus

Microendoscopic probes can be used to investigate deep tissues within the brain and other parts of the body. If sterile surgical techniques are used, long-term imaging studies can be performed on laboratory animals.

MATERIALS

CAUTION: See Appendix 6 for proper handling of materials marked with <!>.
See the end of the chapter for recipes for reagents marked with <R>.

Reagents

Guide Tube Preparation

Ethanol <!>
Glass cleanser for use in sonicator
Optical epoxy adhesive (e.g., NOA 81, Norland Products, Inc.)
Saline, 0.9%

Surgery and Imaging

Agarose, Type III-A (Sigma-Aldrich)
Analgesic (e.g., buprenorphine)
Anesthetic gas (e.g., isoflurane <!>, Southmedic, Inc.) or injectable (e.g., ketamine <!> or xylazine <!>)
Anti-inflammatory (e.g., carprofen <!>, dexamethasone <!>)
Artificial cerebral spinal fluid (ACSF; e.g., from Harvard Apparatus)
Dental acrylic (e.g., Ortho-Jet, Lang Dental Mfg Co., Inc.)
Ethanol, 70%
Eye ointment (e.g., Puralube Vet Ointment, PharmaDerm Nycomed US)
Gel foam
Local anesthetic (e.g., 1%lidocaine)
Mice
Physiologic saline or lactated Ringer's solution (e.g., from Electron Microscopy Sciences)
Skin disinfectant (e.g., betadine, Baxter)
Tissue adhesive (e.g., Vetbond, 3M)

Equipment

Guide Tube Preparation

Coverslips (#0 thickness; e.g., from Electron Microscopy Sciences)
Capillary tubing (e.g., thin-walled glass 1.0–2.5-mm inner diameter, Vitrocom, Inc.)
Culture dishes, sterile for storing assembled guide tubes
Curing light (e.g., COLTOLUX 75, Coltène Whaledent)
Diamond-scribing tool (e.g., from Electron Microscopy Sciences)
Forceps

Glass polisher (e.g., ULTRAPOL, ULTRA TEC Manufacturing, Inc.)
Microdrill (e.g., Osada, Inc. EXL-M40)
Needle, 30 gauge
Sandpaper (fine 500 grit; e.g., 3M)
Sonicator (e.g., Model 1510, Branson Ultrasonics Corp.)
Stereomicroscope (e.g., MZ12.5, Leica)

Surgery and Imaging

Anesthesia system for laboratory animals (e.g., VetEquip Inc. 901806)
Aseptic instruments/surgical tools (e.g., from Fine Science Tools)
Balance (for weighing animals; e.g., Mettler Toledo International, Inc. PG503-S)
Carrier gas tank (e.g., medigrade oxygen from Praxair, Inc.)
Cold light source (e.g., KL 1500, SCHOTT North America, Inc.)
Cotton swabs, sterile
DC temperature regulation system (e.g., FHC Inc. 40-90-8; 40-90-5; 40-90-2-07)
Flexible tape or adhesive dressing (Bioclusive, Johnson and Johnson)
Glass bead sterilizer (e.g., model BS-500, Dent-EQ)
Lens paper
Microendoscope probe (see Imaging Setup)
Microscope (see Imaging Setup)
Microwave (for agarose gel preparation)
Mounting post (custom-made; aluminum 15x 3 x 2-mm bar with 2.7-mm through hole on end)
Mounting-post holder (custom-made; aluminum bar with M2 tapped hole)
Needles, blunt 27- and 29-gauge
Stereotaxic apparatus (custom-made)
Surgical eye spears (e.g., 1556455, Henry Schein Medical)
Waste anesthetic gas system (e.g., VetEquip, Inc. 933101) (optional but recommended)
Waste liquid suction line (custom-made)

EXPERIMENTAL METHOD

Glass Guide Tube Construction (~25 min)

An optically transparent guide tube (Fig. 1D) is often used to assist in delivering the microendoscope to the tissue of interest. Because the tube is sealed at the tip with a small cover glass that permits optical but not physical access to the tissue, microendoscopes can be delivered and can be interchanged with minimal mechanical disturbance to the field of view under inspection. With additional surgical steps to prevent exposure of brain tissue to the external environment, the preparation can also be adapted for long-term time-lapse imaging.

1. Choose a thin-walled capillary glass of appropriate diameter. Typical inner diameters safely exceed the microendoscope diameter by 10%–15%.
2. Cut the thin-walled capillary glass to the desired length. Use a microdrill to uniformly thin the circumference of the glass at the location of the cut. Snap the glass at the thinned portion, and coarsely smooth with the microdrill or sandpaper.
3. Polish one end of the guide tube. Use a fiber-optic polisher or a fine grit sandpaper. Inspect the guide tube end under a stereomicroscope, and ensure flatness. Repolish as necessary.
4. Cut circular pieces of #0-thickness cover glass with diameters matching the outer diameter of the guide tube. Using a diamond scribe, score circular patterns onto the cover glass, and break with the forceps. Tolerances for the cover-glass dimensions are set by the inner and the outer diameters of the guide tube.

5. Clean all glass pieces by sonication while immersed in the cleanser, and store in ethanol until assembly. In subsequent steps, use gloves, and work in a dust-free area.
6. Apply a thin layer of ultraviolet-curing optical adhesive to the polished end of the guide tube. Using a high-magnification stereomicroscope, orient the guide tube toward the objective, and use a fine 30-gauge needle to apply the adhesive onto the guide tube.
7. Attach the circular coverslips to the guide tube. Use forceps to hold the cover glass, and gently drop the coverslip onto the guide tube. Ensure that glue does not enter the central area of the guide tube and that an epoxy seal is formed around the entire circumference of the guide tube. Set the epoxy using an ultraviolet light source.
8. Store guide tubes in clean containers until use (e.g., sterile culture dishes). If possible, allow at least 12 h for the optical epoxy to cure before use. Rinse with saline solution before implantation.

Initial Surgery (~1 h)

The following animal procedures are outlined for the examination of the dorsal hippocampus in adult mice but are applicable to other regions (Fig. 2A,C). All procedures were approved by the Stanford Administrative Panel on Laboratory Animal Care (APLAC). Consultation with those overseeing institutional guidelines for animal surgery care and anesthesia is recommended.

9. Deeply anesthetize mice with isoflurane gas (2.0%–2.5%; mixed with 2-L/min oxygen) or interperitoneal injection of ketamine (75 mg/kg) and xylazine (15 mg/kg). Assess depth of anesthesia by monitoring toe pinch withdrawal, eyelid reflex, and respiration rate.
10. (Optional) Administer dexamethasone (2-mg/kg intramuscular) and carprofen (5-mg/kg subcutaneous) to minimize tissue swelling and inflammation.
11. Secure the animal in a stereotaxic frame. Maintain body temperature at 37°C with a heating blanket. Apply ophthalmic ointment to the eyes.

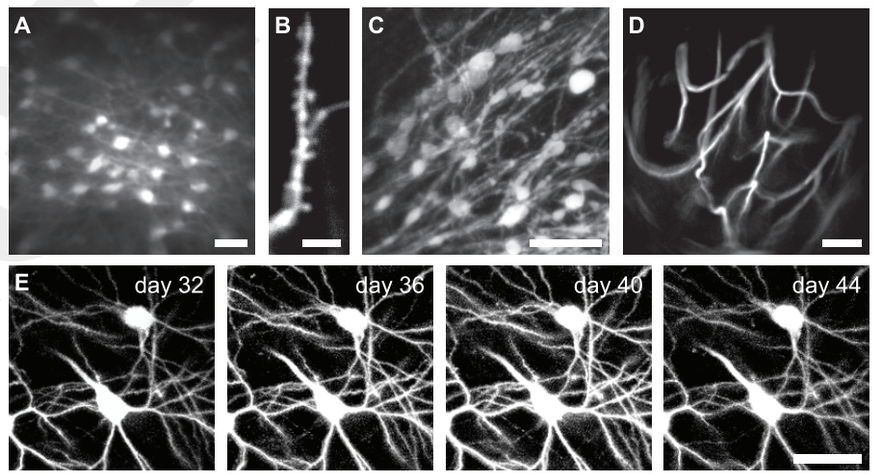

FIGURE 2. Images acquired by fluorescence microendoscopy in live mice. (A) GFP-labeled pyramidal neurons in CA1 hippocampus imaged with a 1-mm singlet probe. Scale bar, 50 μm. (B) High-resolution image of CA1 hippocampal dendritic spines acquired using an LaSFN9 high-resolution probe. Scale bar, 5 μm. (C) GFP-labeled neurons in the brain stem's external cuneate nucleus imaged with a 1-mm doublet probe of 20-mm length and a 0.75-pitch relay. Scale bar, 5 μm. (D) Fluorescein-labeled vasculature in CA1 hippocampus imaged with a 0.5-mm singlet probe. Scale bar, 5 μm. (E) Time-lapse imaging of a GFP-labeled pyramidal neuron in CA1 hippocampus. Scale bar, 40 μm. A–C and E are 2D projections of 3D stacks acquired by two-photon microendoscopy. These stacks were composed of 108 image slices acquired at 2-μm axial separation between adjacent slices for A; nine images with 1.6-μm axial separation for B; 50 images with 0.43-μm axial separation for C; five slices taken at 4.2-μm axial separation for E. D was obtained by one-photon microendoscopy and shows the standard deviation image of a high-speed video sequence of blood flow, which is a postprocessed image that highlights blood vessels.

12. Trim or shave the fur from the top of the head, and disinfect the exposed skin with alternating washes of 70% ethanol and betadine.
13. Expose the cranium in the vicinity dorsal to the brain structure of interest. Remove the periosteum using a probe or a scalpel, and rinse with 0.9% saline solution. After rinsing, use a cotton swab to dry the exposed skull.
14. Apply a thin layer of cyanoacrylate (e.g., Vetbond) to the regions of exposed skull outside of the expected craniotomy site. Use a fine applicator (e.g., hypodermic needle) to spread the cyanoacrylate over the boundaries of the exposed cranium to seal the skin cut sites. Allow the cyanoacrylate to dry for 5 min.
15. Drill a round craniotomy centered over the stereotaxic coordinates of interest (e.g., 2.0-mm posterior and 2.0-mm lateral of the bregma in the hippocampus). A trephine is helpful in marking craniotomy dimensions matched to the microendoscope diameter. Remove the dura with forceps.
16. Perform blunt dissection and aspiration to gradually remove a cylindrical column of neocortical brain tissue with a 27-gauge blunt needle. Continuously irrigate the applied area with sterile ACSF or Ringer's solution. Bleeding from disrupted vasculature is normal, increase irrigation rates to maintain visibility within the column.
17. As the desired imaging area is approached, aspiration with a fine 29-gauge blunt needle can be used to expose the imaging area. Under optimal conditions, a thin layer of tissue remains overlying the cells of interest, to minimize direct mechanical tissue damage from aspiration. In the hippocampal preparation, the overlying corpus callosum can be readily identified by its stereotyped white matter tract patterns.
18. Minimize bleeding from the sides of the aspirated column. This is performed by following applications of saline irrigation and aspiration with 5-sec pause intervals to allow clot formation. Gel foam may be applied to control bleeding. Take care not to allow a clot to form over the imaging area.
19. Optionally, at this step, an animal may be examined for fluorescence labeling, using a low-magnification long working distance objective. (See Imaging below.)
20. Gradually insert a closed-end glass guide tube into the aspirated column. Lower the guide tube until it is in contact with the distal tissue regions. Check that neither air pockets nor bleeding regions are present under the guide tube. If necessary, irrigate with buffer, and repeat guide tube insertion. The tissue should be visible on inspection through the guide tube with a stereomicroscope.
21. Suction any liquids that are present on the cyanoacrylate layer.
22. Apply melted agarose (~1.5%) to the sides of the guide tube, filling gaps between skull and the guide tube. Allow agarose to harden. Excess agarose can be removed by dicing with a scalpel blade.
23. Apply a layer of dental acrylic over all of the exposed skull and sides of the guide tube. Affix a metal connection bar approximately parallel to the plane of the guide tube surface. The distal end of the bar must be at least 1 cm away from the guide tube to prevent obstruction during imaging. Wait 10 min for the acrylic to harden.
24. Affix a piece of flexible tape or adhesive dressing over the guide tube. This will prevent dirt from entering the tube for the duration of time the animal spends in the home cage.
25. Allow the animal to recover from anesthesia. Return mouse to a clean home cage, and maintain heating until righting reflex is shown. Analgesics (e.g., buprenorphine or carprofen) can be administered as necessary.

Imaging Session (>30 min)

26. Reanesthetize mice with isoflurane gas (2.0%–2.5%; mixed with 2-L/min oxygen) or interperitoneal injection of ketamine (75 mg/kg) and xylazine (15 mg/kg). Assess depth of anesthesia by monitoring toe pinch withdrawal, eyelid reflex, and respiration rate.
27. Secure animal into a position suitable for imaging. Use appropriate adaptors to clamp the metal connection bar. Maintain body temperature at 37°C with a heating blanket. Apply ophthalmic ointment to the eyes as necessary.

    See *Troubleshooting*.
28. Insert the microendoscope probe into the guide tube. Remove protective tape to expose the guide tube. Examine the guide tube for any dirt particles. If necessary, deliver H_2O into the guide tube, and rinse. Using air suction through a 25–29-gauge blunt needle, remove all fluid from the guide tube. Take care not to damage the bottom face of the guide tube with excess pressure.
29. Using an eyepiece and bright-field illumination, focus the microscope objective onto the proximal microendoscope surface. Align the microendoscope to the optical axis of the microscope by adjusting the clamp orientation. Under bright-field illumination, a well-aligned microendoscope will appear circular, not elliptical (which would indicate tilt relative to the optical axis).
30. If available, use one-photon fluorescence imaging to locate the desired tissue region. Use the minimal intensity of light necessary to illuminate the tissue. Typically, one gradually adjusts the focal plane of the microscope objective upward (i.e., away from the specimen), assuming that the tissue plane of interest is located closer to the face of the micro-optical objective than to the microendoscope probe's design working distance. Optionally, switch to the two-photon fluorescence mode.

    See *Troubleshooting*.
31. For long-term imaging studies, it is useful to compare images of the specimen obtained in prior imaging sessions. This allows the animal to be reoriented as necessary to optimize the registration of newly acquired images to those taken previously. During the first week following surgery, tissue displacement may occur below the implanted guide tube. In such cases, the microendoscope may need to be translated within the guide tube to assist in alignment with prior images.

    See *Troubleshooting*.
32. Microendoscope probes may be interchanged without displacing the animal by using suction to remove the microendoscope from the glass guide tube.
33. At the end of the experiment, microendoscopes should be cleaned by rinsing and gentle scrubbing with H_2O and lens paper. Guide tubes should be covered with flexible tape, and animals should be returned to their home cages. Monitor animals until righting reflex is shown.

TROUBLESHOOTING

Problem (Step 27): Implants detach during time in the home cage or during the imaging experiment.

Solution: Over the course of a long-term experiment, a small number of implants may detach. Common causes include insufficient drying of the skull or removal of the periosteum preventing proper cyanoacrylate bonding and, in long-term experiments, regrowth of the skin underneath the implant caused by the incomplete application of cyanoacrylate onto the skin–skull interface. Several alternative steps may be performed to address this problem.

1. Substitute Metabond (Parkell) for cyanoacrylate during the application of the thin layer to the skull.
2. Insert two to four miniature stainless-steel screws into the skull to enhance binding of the dental acrylic to the skull. This is a method of last resort, as insertion of screws could result in additional tissue damage.

Problem (Step 30): Excessive tissue motion during imaging.
Solution: Most commonly observed tissue motions are caused by breathing rhythms. First, check the depth of anesthesia during imaging. Second, adjust the head position relative to the animal's trunk to facilitate unconstrained breathing while providing modest mechanical decoupling of the head from motions of the trunk. Another common cause of tissue motion is an excess gap between the tissue and the end of the guide tube; this is the fault of either an improper implantation during the initial surgery or any swelling that occurred then and later subsided. As the brain tissue stabilizes over the course of several days, the guide tube may no longer be optimally positioned for the desired imaging experiment. During implantation, reducing the overall duration of surgery, adjusting the dosage of anti-inflammatory agents, and decreasing the potential heating of the tissue during skull drilling all generally improve experimental quality.

Problem (Step 31): Image quality degrades during image acquisition or across imaging sessions.
Solution: Clean and inspect the microendoscope, and replace it as necessary. Excessive laser power focused to surfaces of the microendoscope can result in damage to the glass. When this occurs, background photon levels in the image typically increase. Inspection of the microendoscope with an epifluorescent microscope will reveal autofluorescent patterns in which laser scanning occurred on the glass surface. Alternatively, image degradation may be an indication of cellular damage. During repeated imaging of subcellular structures such as dendrites or axons, blebbing may appear as well as general fading of fluorescence in the scanned regions across the imaging sessions. In such cases, use lower intensity illumination. As an alternative to acquiring a single image at a higher illumination power, averaging of multiple images each taken at a faster acquisition speed and lower power may also improve image quality.

DISCUSSION

Optical microendoscopy is suited for cellular level imaging deep within tissue in live animals or humans. Researchers can choose among a wide variety of microendoscope probe designs to select those best matched to their needs. For the combined acquisition of high-speed videos and 3D image stacks from the same specimen, it is useful to have a microscope that allows online toggling between one-photon fluorescence and laser-scanning imaging (Jung et al. 2004) (Fig. 1A). Laser-scanning second-harmonic generation microendoscopy can generally be performed on any microscope intended for intravital two-photon imaging by an appropriate choice of emission filter (Llewellyn et al. 2008). Overall, microendoscopy is a flexible technique that can be used with multiple modes of contrast generation, at different tissue depths, and with a wide variety of imaging parameters. In the brain, this flexibility has enabled the examination of intracellular calcium dynamics, microcirculatory flow, and neuronal morphology. Because the microendoscope is conceptually, at the core, an optical relay, any fluorescent marker that performs well under conventional one- or two-photon fluorescence microscopy will generally perform comparably well under microendoscopy in similar optical conditions.

Comparison to Other Strategies for Imaging Deep Tissues

Some deep structures may be accessed by conventional microscope optics. In one strategy, more invasive aspiration of the tissue allows direct access to the tissue of interest (Mizrahi et al. 2004). A

wide column of tissue must be removed to prevent blocking light to and from the specimen if imaging with a high NA is to be achieved. The applicability of this technique seems limited because deeper structures require surgery and aspiration that are substantially more invasive.

A second strategy for deep imaging extends the penetration depth of conventional two-photon microscopy to tissues as deep as 1 mm below the surface, as reviewed in Wilt et al. (2009). To achieve this, several methods exist to improve fluorescence generation, including the use of illumination sources with higher pulse energies and longer wavelengths and adaptive optics to improve the focusing of light in the tissue. In addition to providing a relatively noninvasive means of imaging structures at intermediate depths, such as the infragranular layers of the neocortex, these improvements are also compatible with microendoscopy. However, because of the exponential increase with the depth of a photon's probability of being scattered, these methods for extending the reach of conventional light microscopy are unlikely to reach the tissue depths of several millimeters to ~1 cm that have already been shown by microendoscopy.

A Chronic Mouse Preparation for Time-Lapse Microendoscopy

The implantation of sealed optical guide tubes into the brain enables a chronic rodent preparation for repeated imaging of the same tissue sites over extended time periods of ~2 mo or more. In some cases, we have been able to perform imaging for up to 1 yr after surgery. Thus, longitudinal imaging studies can be performed over timescales sufficiently long to monitor the imaging field over the course of a disease, acquisition of a behavioral response, or a significant portion of the animal's adult life.

A key advantage of implanting guide tubes for long-term time-lapse imaging is that the effects of surgery can be temporally separated from subsequent imaging sessions. By comparison, during acute preparations for hippocampal imaging (Mizrahi et al. 2004), aspiration of overlying neocortical tissue can result in bleeding into the field of view, potentially degrading image quality or optically obscuring targets of interest. As with the use of implanted cranial windows (Holtmaat et al. 2009), the postponement of imaging for up to ~2 wk after surgery results in a lasting improvement in image quality. Any short-term effects of surgical anesthesia on the tissue can also be circumvented by using other or briefer-lasting anesthetics during imaging or by bypassing anesthesia altogether when imaging in awake animals.

The use of implanted guide tubes also implies multiple microendoscopes can be used to inspect the same tissue site without mechanically disturbing the tissue in both acute and long-term experiments. Low-magnification microendoscopes that are used to locate regions of interest can be exchanged for microendoscopes of higher resolution over a smaller field of view. Individual animal subjects can be repeatedly inspected and under different conditions while anesthetized, can be alert but restrained or can be allowed to behave freely.

Limitations

Microendoscopy opens new possibilities for imaging in deep brain areas, but researchers should also consider the limitations of our time-lapse methodology. The implantation of imaging guide tubes necessarily perturbs the brain. We minimize the impact of such perturbations by placing the guide tubes outside, not within, the tissue being imaged. Alternative approaches, such as implanting a microendoscope with a microprism for sideways viewing of the tissue adjacent to the insertion path (Murayama et al. 2007), or gradually inserting a microendoscope over days akin to how electrodes are often inserted in chronic electrophysiological recordings, may also be a viable means of minimizing perturbations to the imaged tissue. Our own histological studies have shown that guide tube implantation leads to a thin ~25–40-μm layer of glial activation surrounding the implant. As with implantation of glass cranial windows for intravital microscopy (Xu et al. 2007), glial activation generally declines over time and does not impede imaging of the tissue lying beyond the activated layer. Nevertheless, researchers should design studies that carefully separate any putative effects of imaging and surgical procedures from those of the experimental manipulation. For example, individual

animals can be implanted with guide tubes at symmetric stereotactic coordinates in opposing hemispheres, permitting one imaging site to provide control data while the opposing site undergoes an experimental manipulation. The experimental manipulation might involve, for example, lesion, electrophysiological, pharmacological, viral, or optogenetic strategies for manipulating tissue. In such a controlled design, each animal would provide data to both the control and the experimental groups, and the subjects in each group would be inherently matched in age, experimental schedule, and sex.

CONCLUSION

In conclusion, microendoscopy is a useful technique for expanding the range of tissues accessible to cellular level imaging in live animals or humans. Microendoscope probe designs can be customized to accommodate a wide range of imaging situations. Chronic implantation of imaging guide tubes enables long-term time-lapse imaging studies and permits multiple microendoscope probes to be easily exchanged for inspecting the same tissue site at different magnifications. Experimental designs should control for putative effects on the brain of the implantation and imaging procedures, separating these from the effects of the experimental manipulation. Overall, microendoscopy opens a wide range of possibilities for imaging cells in brain areas outside the reach of conventional light microscopy, for basic research purposes, studies of animal disease models, or testing of new therapeutics.

ACKNOWLEDGMENTS

This work was supported by the Stanford Biophysics training grant to RPJB from the U.S. National Institutes of Health and research funding provided to M.J.S. under the National Institute on Drug Abuse Cutting-Edge Basic Research Awards(NIDA CEBRA) DA017895, the National Institute of Neurological Disorders and Stroke (NINDS) R01NS050533, and the National Cancer Institute (NCI) P50CA114747. We thank our collaborators Bernhard Messerschmidt of Grintech GmbH and Tony Ko, Juergen C. Jung, Alessio Attardo, Yaniv Ziv, Michael Llewellyn, Scott Delp, George Capps, Alison Waters, Tammy J. Wang, and Lawrence Recht of Stanford University for their contributions to the methodologies summarized here.

REFERENCES

Barretto RP, Messerschmidt B, Schnitzer MJ. 2009. In vivo fluorescence imaging with high-resolution microlenses. Nat Methods 6: 511–512.

Barretto RP, Ko TH, Jung JC, Wang TJ, Capps G, Waters AC, Ziv Y, Attardo A, Recht L, Schnitzer MJ. 2010. Time-lapse imaging of disease progression in deep brain areas using fluorescence microendoscopy.

Dombeck DA, Khabbaz AN, Collman F, Adelman TL, Tank DW. 2007. Imaging large-scale neural activity with cellular resolution in awake, mobile mice. Neuron 56: 43–57.

Engelbrecht CJ, Johnston RS, Seibel EJ, Helmchen F. 2008. Ultra-compact fiberoptic two-photon microscope for functional fluorescence imaging in vivo. Opt Express 16: 5556–5564

Flusberg BA, Cocker ED, Piyawattanametha W, Jung JC, Cheung EL, Schnitzer MJ. 2005. Fiber-optic fluorescence imaging. Nat Methods 2: 941–950.

Flusberg BA, Nimmerjahn A, Cocker ED, Mukamel EA, Barretto RP, Ko TH, Burns LD, Jung JC, Schnitzer MJ. 2008. High-speed, miniaturized fluorescence microscopy in freely moving mice. Nat Methods 5: 935–938.

Gobel W, Helmchen F. 2007. In vivo calcium imaging of neural network function. Physiology 22: 358–365.

Gobel W, Kerr JN, Nimmerjahn A, Helmchen F. 2004. Miniaturized two-photon microscope based on a flexible coherent fiber bundle and a gradient-index lens objective. Opt Lett 29: 2521–2523.

Helmchen F, Denk W. 2005. Deep tissue two-photon microscopy. Nat Methods 2: 932–940.

Holtmaat A, Svoboda K. 2009. Experience-dependent structural synaptic plasticity in the mammalian brain. *Nat Rev Neurosci* **10:** 647–658.

Holtmaat A, Bonhoeffer T, Chow DK, Chuckowree J, De Paola V, Hofer SB, Hubener M, Keck T, Knott G, Lee WC, et al. 2009. Long-term, high-resolution imaging in the mouse neocortex through a chronic cranial window. *Nat Protoc* **4:** 1128–1144.

Jung JC, Schnitzer MJ. 2003. Multiphoton endoscopy. *Opt Lett* **28:** 902–904.

Jung JC, Mehta AD, Aksay E, Stepnoski R, Schnitzer MJ. 2004. In vivo mammalian brain imaging using one- and two-photon fluorescence microendoscopy. *J Neurophysiol* **92:** 3121–3133.

Kerr JN, Denk W. 2008. Imaging in vivo: Watching the brain in action. *Nat Rev Neurosci* **9:** 195–205.

Levene MJ, Dombeck DA, Kasischke KA, Molloy RP, Webb WW. 2004. In vivo multiphoton microscopy of deep brain tissue. *J Neurophysiol* **91:** 1908–1912.

Llewellyn ME, Barretto RP, Delp SL, Schnitzer MJ. 2008. Minimally invasive highspeed imaging of sarcomere contractile dynamics in mice and humans. *Nature* **454:** 784–788.

Mehta AD, Jung JC, Flusberg BA, Schnitzer MJ. 2004. Fiber optic in vivo imaging in the mammalian nervous system. *Curr Opin Neurobiol* **14:** 617–628.

Mizrahi A, Crowley JC, Shtoyerman E, Katz LC. 2004. High-resolution in vivo imaging of hippocampal dendrites and spines. *J Neurosci* **24:** 3147–3151.

Mukamel EA, Nimmerjahn A, Schnitzer MJ. 2009. Automated analysis of cellular signals from large-scale calcium imaging data. *Neuron* **63:** 747–760.

Murayama M, Perez-Garci E, Luscher HR, Larkum ME. 2007. Fiberoptic system for recording dendritic calcium signals in layer 5 neocortical pyramidal cells in freely moving rats. *J Neurophysiol* **98:** 1791–1805.

Nimmerjahn A, Mukamel EA, Schnitzer MJ. 2009. Motor behavior activates Bergmann glial networks. *Neuron* **62:** 400–412.

Rochefort NL, Jia H, Konnerth A. 2008. Calcium imaging in the living brain: Prospects for molecular medicine. *Trends Mol Med* **14:** 389–399.

Wilt BA, Burns LD, Wei Ho ET, Ghosh KK, Mukamel EA, Schnitzer MJ. 2009. Advances in light microscopy for neuroscience. *Annu Rev Neurosci* **32:** 435–506.

Xu HT, Pan F., Yang G, Gan WB. 2007. Choice of cranial window type for in vivo imaging affects dendritic spine turnover in the cortex. *Nat Neurosci* **10:** 549–551.